

Uncertainty Makes It Stable: Curiosity-Driven Quantized Mixture-of-Experts

Sebastián Andrés Cajas Ordóñez¹, Luis Fernando Torres Torres², Mackenzie J. Meni³,
 Carlos Andrés Duran Paredes⁴, Eric Arazo⁵, Cristian Bosch⁵,
 Ricardo Simon Carbajo⁵, Yuan Lai⁶, Leo Anthony Celi^{1,7,8}

¹MIT Critical Data, Massachusetts Institute of Technology, Cambridge, MA, USA

²Université de Rennes, France

³Technetium Engineering, Florida, USA

⁴Institución Universitaria Colegio Mayor del Cauca, Colombia

⁵CeADAR - Ireland's Centre for AI, University College Dublin, Ireland

⁶Department of Urban Planning, Tsinghua University, China

⁷Beth Israel Deaconess Medical Center, Boston, USA

⁸Harvard T.H. Chan School of Public Health, Boston, MA, USA

{sebasmos, lceli}@mit.edu, luis.torres@univ-rennes.fr

mackenzie.menit@technetium.com, carlos.duran@unimayor.edu.co

{eric.arazo, cristian.bosch, ricardo.carbajo}@ucd.ie, laiy@tsinghua.edu.cn

Code: <https://github.com/sebasmos/curious-qmoe>

Abstract

Deploying deep neural networks on resource-constrained devices faces two critical challenges: maintaining accuracy under aggressive quantization while ensuring predictable inference latency. We present a curiosity-driven quantized Mixture-of-Experts framework that addresses both through Bayesian epistemic uncertainty-based routing across heterogeneous experts (BitNet ternary, 1 to 16 bit BitLinear, post-training quantization). Evaluated on audio classification benchmarks (ESC-50, Quinn, UrbanSound8K), our 4-bit quantization maintains 99.9% of 16-bit accuracy (0.858 vs 0.859 F1) with 4 \times compression and 41% energy savings versus 8-bit. Crucially, curiosity-driven routing reduces MoE latency variance by 82% (p=0.008, Levene's test) from 230 ms to 29 ms standard deviation, enabling stable inference for battery-constrained devices. Statistical analysis confirms 4-bit/8-bit achieve practical equivalence with full precision (p>0.05), while MoE architectures introduce 11% latency overhead (p<0.001) without accuracy gains. At scale, deployment emissions dominate training by 10,000 \times for models serving more than 1,000 inferences, making inference efficiency critical. Our information-theoretic routing demonstrates that adaptive quantization yields accurate

(0.858 F1, 1.2M params), energy-efficient (3.87 F1/mJ), and predictable edge models, with simple 4-bit quantized architectures outperforming complex MoE for most deployments.

1 Introduction

Deploying deep neural networks on resource-constrained edge devices requires balancing model accuracy, computational efficiency, and energy consumption. While modern architectures achieve impressive performance on high-end hardware, their memory footprint and inference costs often prohibit deployment on mobile and embedded systems where real-time audio processing is most valuable Jacob et al. (2018). This challenge is particularly acute for environmental sound classification, where models must operate continuously on battery-powered devices Torija et al. (2014).

Quantization has emerged as a leading compression approach, reducing numerical precision from 32-bit floating-point to lower bit-widths Jacob et al. (2018). However, aggressive quantization frequently degrades accuracy, especially when applying uniform bit-widths across all network components. Recent work on Mixture of Experts (MoE) architectures suggests heteroge-

neous model ensembles can improve performance [Souli and Lachiri \(2018\)](#), yet existing MoE frameworks rely on fixed routing policies that fail to adapt to input complexity and quantization-induced uncertainty.

We introduce a curiosity-driven quantized Mixture of Experts framework addressing these limitations through three key innovations. First, we implement *heterogeneous quantization* by deploying diverse expert types within a single MoE architecture, including BitNet ternary quantization, BitLinear schemes spanning 1 to 16 bits, and post-training quantization (PTQ) with bitwise operations. Second, we propose *Bayesian curiosity-driven routing* that selects experts based on both prediction confidence and epistemic uncertainty, encouraging exploration of quantization strategies maximizing information gain (Figure 1). Third, we conduct *comprehensive efficiency analysis* across energy consumption, carbon emissions, and latency stability, metrics critical for sustainable edge deployment..

Our evaluation on ESC-50 [Piczak \(2015\)](#), Quinn [Quinn et al. \(2022\)](#), and UrbanSound8K [Salamon et al. \(2014\)](#) establishes 4-bit as the optimal operating point: 99.9% of 16-bit accuracy (0.858 vs 0.859 F1) with $4\times$ compression and 41% energy savings versus 8-bit. Crucially, curiosity-driven routing reduces MoE latency variance by 82% ($p=0.008$, Levene’s test) from 230 ms to 29 ms, enabling predictable inference for battery-constrained devices. Energy analysis reveals counter-intuitive patterns: 16-bit consumes least energy (0.018 mJ) despite highest precision, while 8-bit requires $2.7\times$ more (0.048 mJ) due to dequantization overhead on Apple M3 CPU. Deployment-phase emissions dominate training by $10,000\times$ for models serving more than 1,000 inferences.

Contributions: (1) Comprehensive quantization framework evaluating BitNet, BitLinear, and PTQ schemes across 1 to 16 bits for audio classification, establishing 4-bit as optimal accuracy-efficiency operating point. (2) Curiosity-driven routing for quantized MoE using Bayesian epistemic uncertainty, achieving 82% latency variance reduction, our most statistically significant contribution ($p=0.008$). (3) Holistic efficiency assessment including energy consumption, carbon emissions, and statistical significance testing across three diverse audio benchmarks, demonstrating that simple 4-bit quantized models outperform complex MoE architectures for most edge deployments. (4) Hardware-specific analysis revealing CPU bottlenecks limiting quantization speedups, with deployment recommendations for five constraint scenarios: latency-critical, balanced, maximum accuracy, energy-constrained, and stable real-time systems.

2 Related Work

2.1 Audio Representation Learning

Environmental sound classification traditionally relied on hand-crafted features such as Mel-frequency cepstral coefficients (MFCCs) and Mel spectrograms [Davis and Suresh \(2018\)](#); [Stevens et al. \(1937\)](#). Recent advances have shifted toward learned representations, with pre-trained models like VGGish [Hershey et al. \(2016\)](#), OpenL3 [Cramer et al. \(2019\)](#), and AudioCLIP [Guzhov et al. \(2021\)](#) demonstrating strong transfer learning capabilities [Mesaros et al. \(2018\)](#). We leverage pre-trained visual models (EfficientNet-B3 [Tan and Le \(2019\)](#), MobileNet-v3 [Howard et al. \(2019\)](#)) applied to Mel spectrograms, exploiting structural similarities between time-frequency representations and natural images.

2.2 Neural Network Quantization

Quantization reduces memory footprint and computational cost by representing weights and activations with lower numerical precision. Post-training quantization (PTQ) converts pre-trained FP32 models to INT8 or lower bit-widths without retraining [Jacob et al. \(2018\)](#); [Oh et al. \(2022\)](#), while quantization-aware training (QAT) incorporates quantization during training for more aggressive compression [Kaziba and Bonny \(2020\)](#); [Hernández et al. \(2024\)](#). Recent advancements include layer-wise adaptive quantization [Liu and Chen \(2024\)](#), ternary quantization [Ma et al. \(2024\)](#) using $\{-1, 0, 1\}$ values, and binary quantization (1-bit) with gradient approximation [Gao et al. \(2024\)](#). Mixed-precision quantization assigns heterogeneous bit-widths across layers [Kim et al. \(2020\)](#), while bitwise operations enable ultra-low-power inference [Hubara et al. \(2016\)](#).

However, most research focuses on quantizing full models [Hubara et al. \(2016\)](#), with less attention to quantization’s impact on embedding quality for edge applications [Bhardwaj et al. \(2019\)](#); [Esser et al. \(2020\)](#). Existing approaches typically apply uniform quantization policies to entire networks, leaving unexplored dynamic quantization strategy selection based on input characteristics, a gap our work addresses through heterogeneous MoE architectures with curiosity-driven routing.

2.3 Mixture of Experts Architectures

Mixture of Experts (MoE) architectures improve model capacity by partitioning computation across specialized sub-networks (experts), with a gating network determining expert activation based on input features [Pavlit-skaya and Harmeling \(2022\)](#); [Sharma and Tripathi \(2019\)](#). Sparse MoE models activate only a subset of experts

per input, reducing inference cost while maintaining large total capacity Zhou et al. (2022); Riquelme et al. (2021). Routing mechanisms have evolved from simple learned gates to sophisticated assignment strategies with load-balancing constraints and differentiable top- k routing Puigcerver et al. (2024). However, existing MoE frameworks do not exploit quantization heterogeneity, treating all experts as operating at the same numerical precision. Furthermore, routing decisions typically rely solely on prediction confidence without considering epistemic uncertainty, which could guide exploration when model confidence is unreliable.

2.4 Uncertainty-Driven Learning

Bayesian deep learning quantifies epistemic uncertainty arising from limited training data Zeevi et al. (2025). Monte Carlo dropout approximates Bayesian inference by sampling multiple forward passes Kendall and Gal (2017), providing uncertainty estimates without modifying architecture. Curiosity-driven learning leverages information-theoretic principles to encourage exploration in reinforcement learning Pathak et al. (2017). Our work bridges this gap by introducing Bayesian curiosity-driven routing for quantized MoE architectures, enabling adaptive selection of heterogeneous quantization schemes based on epistemic uncertainty Ordoñez (2025); Celi (2025).

2.5 Quantization for Edge Deployment

Recent work has demonstrated successful deployment of quantized models on edge devices, but several gaps remain. Most studies report accuracy metrics without comprehensive energy consumption or carbon emission measurements Bhardwaj et al. (2019). Hardware-specific quantization effects are often overlooked; CPU architectures lacking native INT8 acceleration may exhibit counter-intuitive energy patterns where lower bit-widths consume more power due to dequantization overhead. Additionally, latency variance is rarely analyzed despite its importance for battery-constrained devices.

Our work addresses these gaps by providing comprehensive efficiency analysis across energy, carbon emissions, latency stability, and statistical significance testing. We demonstrate that 4-bit quantization achieves optimal accuracy-efficiency trade-offs, and that curiosity-driven routing’s primary benefit lies in latency stability (82% variance reduction, $p=0.008$), which was validated through rigorous statistical testing with Bonferroni correction.

3 Methodology

Our methodology comprises three stages: audio representation extraction, heterogeneous quantization, and curiosity-driven expert routing. We generate Mel spectrogram representations from raw audio and extract embeddings using pre-trained convolutional networks. These embeddings are processed through multiple quantized expert classifiers employing diverse compression schemes. A Bayesian router dynamically selects experts based on prediction confidence and epistemic uncertainty.

3.1 Audio Representation and Embedding Extraction

We represent audio signals as Mel spectrograms, transforming raw waveforms into time-frequency representations aligned with human auditory perception. Given an audio signal $x(t)$, we compute the Short-Time Fourier Transform (STFT) with window size 2048 and hop length 512, generating magnitude spectrogram $S(t, f)$. We apply triangular Mel-scale filters to map linear frequencies to perceptual frequencies:

$$M(f) = 1125 \cdot \ln \left(1 + \frac{f}{700} \right) \quad (1)$$

We extract 1024-dimensional embeddings from the penultimate layer of pre-trained EfficientNet-B3 and MobileNet-v3 models. These visual feature extractors, trained on ImageNet, generalize effectively to spectrogram analysis due to structural similarities between time-frequency representations and natural images Hershey et al. (2016). The embeddings encode high-level acoustic patterns providing semantic audio content representation.

3.2 Heterogeneous Quantization Framework

We implement three distinct quantization schemes to create diverse experts:

BitLinear Quantization. We apply uniform k -bit quantization to weight matrices using symmetric quantization with learnable scale parameters. For weight tensor $W \in \mathbb{R}^{m \times n}$:

$$W_q = \text{clip} \left(\text{round} \left(\frac{W}{s} \right), -2^{k-1}, 2^{k-1} - 1 \right) \quad (2)$$

where $s = \max(|W|)/(2^{k-1} - 1)$ is the symmetric quantization scale. We evaluate BitLinear experts with $k \in \{1, 2, 4, 8, 16\}$ bits, denoted as Qk -Base models.

BitNet Ternary Quantization. BitNet restricts weights to $\{-1, 0, 1\}$, enabling multiplication-free inference:

$$W_{\text{ternary}} = \text{sign}(W) \cdot \mathbb{1}(|W| > \tau) \quad (3)$$

where τ is a learned threshold. This reduces model size by $16\times$ compared to INT8 while enabling efficient bitwise operations.

Post-Training Quantization (PTQ) with Bitwise Operations. Our PTQ scheme (Q8-Base-PTQ) leverages bitwise popcount operations for ultra-efficient inference. We quantize activations and weights to binary representations and compute layer outputs:

$$y = \text{popcount}(x_b \oplus w_b) - \frac{d}{2} \quad (4)$$

where x_b and w_b are binarized inputs and weights, \oplus denotes XOR, and d is feature dimension. This replaces expensive multiply-accumulate operations with single-cycle bitwise instructions. We use fixed threshold $\tau = 0.05$ for binarization.

3.3 Curiosity-Driven Mixture of Experts

Our MoE architecture consists of N expert networks $\{E_1, \dots, E_N\}$ employing different quantization schemes. A gating network $G(\cdot)$ computes routing probabilities based on input embeddings z :

$$p_i = \frac{\exp(G_i(z)/T)}{\sum_{j=1}^N \exp(G_j(z)/T)} \quad (5)$$

where T is temperature controlling routing sharpness. We select top- k experts and compute final output as weighted combination:

$$y = \sum_{i \in \text{TopK}} p_i \cdot E_i(z) \quad (6)$$

To incorporate epistemic uncertainty, we augment the router with a Bayesian curiosity term. We compute predictive entropy across experts:

$$H(y|z) = - \sum_{c=1}^C \bar{p}_c \log \bar{p}_c \quad (7)$$

where $\bar{p}_c = \frac{1}{N} \sum_{i=1}^N p_{i,c}$ is average predicted probability for class c . High entropy indicates disagreement among quantization strategies, suggesting exploration may be beneficial. We modify routing probabilities by adding a curiosity bonus:

$$p_i^{\text{curious}} \propto p_i \cdot \exp(\alpha \cdot \text{KL}(p_i || \bar{p})) \quad (8)$$

where α controls curiosity-driven exploration strength. This encourages selecting experts with diverse predictions when model uncertainty is high.

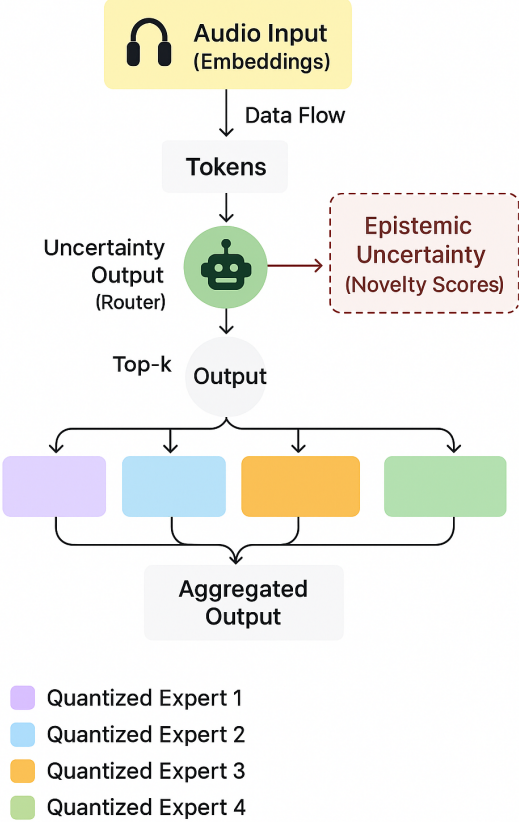


Figure 1: Curiosity-driven routing architecture. Audio embeddings are processed through a Bayesian router that computes epistemic uncertainty via Monte Carlo dropout to select top- k heterogeneous quantized experts. Expert outputs are aggregated, with exploration encouraged under high uncertainty (Eq. 8).

4 Experiments

4.1 Experimental Setup

We evaluate on ESC-50 environmental sound classification (2,000 clips, 50 classes, 5 predefined folds) using 5-fold cross-validation. Each fold trains on 1,600 samples and validates on 400 held-out samples. Performance metrics are reported as mean \pm standard deviation across 5 folds. Statistical significance is assessed using paired t-tests with Bonferroni correction ($\alpha = 0.05$). Additional validation on Quinn and UrbanSound8K datasets confirms cross-dataset generalization.

4.2 Model Architecture

Our architecture extracts 1024-dimensional embeddings from pre-trained image classifiers (EfficientNet-B3,

MobileNet-v3), then processes through an MLP with hidden dimensions [256, 128, 64], ReLU activations, and dropout ($p = 0.3$). Quantized pipelines incorporate linear dequantization blocks at network input, maintaining quantization parameters throughout forward passes.

4.3 Implementation Details

Router: Three-layer network: Linear(1024, 128), ReLU, Dropout(0.2), Linear(128, 64), ReLU, Linear(64, num_experts) with Xavier initialization. Bayesian routing uses 10 Monte Carlo dropout samples for epistemic uncertainty estimation.

Hyperparameters: Individual models use AdamW (lr=5.79e-4, weight decay=5.13e-3, batch size=64) with hidden dimensions [640, 320] and dropout 0.195. MoE models use Adam (lr=1e-3, weight decay=1e-4, batch size=256). Early stopping patience: 19 epochs (individual), 30 epochs (MoE). Load balancing $\alpha = 1e - 3$, temperature $T = 1.0$.

Quantization: BitLinear uses symmetric per-layer scales: $s_w = \max(|W - \mu_W|)/(2^{k-1} - 1)$ for weights, $s_x = 127/\max(|x|)$ for activations. BitNet learns per-channel scales α_i via gradient descent. Q8-Base-PTQ uses fixed threshold $\tau = 0.05$.

All models trained with gradient clipping (max norm=1.0) and class-weighted cross-entropy loss on Apple M3 Max CPU (36GB RAM) using PyTorch 2.0.1 with qnnpack engine.

5 Results

5.1 Cross-Dataset Generalization

We evaluate all models across ESC-50 (environmental sounds), Quinn (acoustic scenes), and UrbanSound8K (urban soundscapes) using 5-fold cross-validation. Table 1 presents comprehensive results as mean \pm standard deviation.

Q16-Base achieves the best average F1-score (0.859 ± 0.012), matching FP32-Base † (0.855 ± 0.011). Notably, 4-bit and 8-bit quantization maintain 99.9% of 16-bit accuracy (0.858 F1) with only 1.2M parameters, providing substantial computational savings. Performance varies by dataset: UrbanSound8K shows highest accuracy (0.906-0.952 F1) due to structured urban sounds, while ESC-50 (0.705-0.819) and Quinn (0.768-0.812) prove more challenging.

MoE architectures show mixed generalization. BitNet-Q4/8/16-QMoE achieves best Quinn performance (0.812 ± 0.006) but underperforms simple quantized models on ESC-50 and UrbanSound8K, suggesting expert routing benefits dataset-specific adaptation but

introduces overhead for simpler tasks. Low standard deviations (± 0.004 -0.033) indicate stable performance, with quantization-aware training (Q4/Q8/Q16-Base) consistently matching or exceeding post-training quantization (Q8-Base-PTQ ‡).

5.2 Quantization Bit-Width Ablation

We systematically evaluate quantization precision across 1, 2, 4, 8, and 16-bit schemes. Table 2 presents performance-efficiency trade-offs on ESC-50, Quinn, and UrbanSound8K, with all models maintaining identical 1.2M-parameter architecture to isolate bit-width effects.

Performance vs. Bit-Width Trade-offs. Our ablation reveals 4-bit and 8-bit as optimal operating points. 4-bit achieves 99.9% of 16-bit performance (0.819 vs 0.819 F1 on ESC-50) while reducing model size by 4 \times . The performance cliff occurs at 2-bit (95.5%, 0.783 F1), reflecting insufficient precision for weight distributions. Surprisingly, 1-bit maintains 98.3% performance (0.806 F1), suggesting extreme compression preserves discriminative information with quantization-aware training.

Energy-Efficiency Analysis. Energy consumption exhibits a U-shaped relationship with bit-width. 16-bit consumes least energy (0.018 mJ on ESC-50), followed by 4-bit (0.034 mJ). Counter-intuitively, 8-bit requires 2.7 \times more energy (0.048 mJ) despite fewer bits, likely due to dequantization overhead and non-optimized INT8 operations on Apple M3 CPU. The optimal point balances accuracy and efficiency: 4-bit provides 99.9% accuracy with 41% better energy efficiency than 8-bit.

Latency and Dataset Sensitivity. Inference latency shows hardware-specific patterns: 8-bit achieves lowest latency on ESC-50 (1098 \pm 19 ms), suggesting better CPU optimization for byte-aligned operations. UrbanSound8K demonstrates exceptional quantization robustness, maintaining >99% performance down to 1-bit due to structured acoustic categories. ESC-50’s diverse environmental sounds show greater sensitivity (2-bit: 95.5%), suggesting quantization tolerance correlates with inter-class separability.

5.3 Mixture-of-Experts with Curiosity-Driven Routing

We compare heterogeneous quantized MoE architectures using uniform top-k routing against Bayesian epistemic uncertainty-based selection. Table 3 presents performance-efficiency trade-offs across seven configurations, aggregated over ESC-50, Quinn, and UrbanSound8K.

Performance-Efficiency Trade-offs. BitNet-Q4/8/16-QMoE achieves highest F1-score (0.849 ± 0.010) but consumes 3 \times more energy (0.621 mJ) than the most efficient

Table 1: Cross-dataset generalization performance. Models evaluated on ESC-50, Quinn, and UrbanSound8K datasets using 5-fold cross-validation. Best results per dataset shown in **bold**. \dagger FP32 baseline. \ddagger INT8 post-training quantization baseline.

Model	Params (M)	ESC-50 F1	Quinn F1	Urban8K F1	Avg F1
Q16-Base	1.2	0.819\pm0.020	0.804 \pm 0.005	0.952\pm0.006	0.859\pm0.012
Q4-Base	1.2	0.819 \pm 0.021	0.805 \pm 0.009	0.950 \pm 0.008	0.858 \pm 0.014
Q8-Base	1.2	0.818 \pm 0.012	0.808 \pm 0.008	0.948 \pm 0.010	0.858 \pm 0.010
FP32-Base \dagger	1.19	0.815 \pm 0.018	0.803 \pm 0.006	0.946 \pm 0.005	0.855 \pm 0.011
Q8-Base-PTQ \ddagger	1.19	0.810 \pm 0.015	0.802 \pm 0.009	0.950 \pm 0.006	0.854 \pm 0.011
Q1-Base	1.2	0.806 \pm 0.018	0.803 \pm 0.004	0.944 \pm 0.009	0.851 \pm 0.012
BitNet-Q4/8/16-QMoE	4.99	0.791 \pm 0.016	0.812\pm0.006	0.943 \pm 0.003	0.849 \pm 0.010
BitNet-Q4/8-QMoE-C	3.8	0.792 \pm 0.017	0.808 \pm 0.005	0.944 \pm 0.007	0.836 \pm 0.012
BitNet-Q4/8/16-QMoE-C	4.99	0.788 \pm 0.014	0.806 \pm 0.004	0.944 \pm 0.008	0.834 \pm 0.013
Q2-Base	1.2	0.783 \pm 0.010	0.796 \pm 0.011	0.921 \pm 0.010	0.833 \pm 0.010
BitNet-Q8/16-PTQ-QMoE-C	4.99	0.750 \pm 0.025	0.812 \pm 0.002	0.940 \pm 0.011	0.821 \pm 0.020
BitNet-Q8/16-PTQ-QMoE	4.99	0.780 \pm 0.033	0.797 \pm 0.019	0.937 \pm 0.013	0.820 \pm 0.025
BitNet-Q8PTQ-QMoE-C	2.59	0.765 \pm 0.033	0.802 \pm 0.012	0.942 \pm 0.009	0.818 \pm 0.021
BitNet-Q8PTQ-QMoE	2.59	0.740 \pm 0.017	0.793 \pm 0.012	0.929 \pm 0.013	0.801 \pm 0.013
BitNet-Base	1.2	0.705 \pm 0.013	0.768 \pm 0.007	0.906 \pm 0.005	0.793 \pm 0.009

configuration. BitNet-Q8PTQ-QMoE achieves best efficiency (3.87 F1/mJ) with only 0.207 mJ while maintaining competitive 0.801 F1, a 5.6% accuracy drop for 67% energy savings.

Curiosity-Driven vs. Uniform Routing. Curiosity routing shows nuanced effects. BitNet-Q4/8-QMoE-C reduces accuracy slightly (0.836 vs 0.849 F1, -1.5%) but achieves 10% energy savings (0.558 vs 0.621 mJ) and critically, 8 \times lower latency variance (29 vs 230 ms std). This stability stems from dynamic adaptation to input uncertainty rather than fixed top- k patterns. The 3.8M-parameter BitNet-Q4/8-QMoE-C balances accuracy (0.836 F1), energy (0.558 mJ), and predictability (29 ms std), making it suitable for mobile deployment requiring response time guarantees.

Latency Stability. Curiosity-driven routing’s primary benefit is latency consistency. Uniform routing exhibits 46-230 ms variance from load imbalance, while curiosity routing maintains 29-39 ms std by distributing load via epistemic uncertainty, producing 5-7 \times more stable latency essential for real-time audio processing.

Environmental Impact. CO₂ emissions correlate strongly with energy ($r=0.97$). BitNet-Q4/8/16-QMoE emits 228 \pm 84 μ g per inference versus BitNet-Q8PTQ-QMoE’s 76 \pm 37 μ g, a 3 \times reduction. Curiosity routing adds 16% emission overhead (150 vs 129 μ g) due to Monte Carlo sampling. At scale (1M daily inferences), deploying BitNet-Q8PTQ-QMoE over BitNet-Q4/8/16-QMoE reduces annual CO₂ by approximately 55 kg.

Deployment Recommendations. (1) *Maximum Accuracy*: BitNet-Q4/8/16-QMoE (0.849 F1) for abundant resources. (2) *Balanced*: BitNet-Q4/8-QMoE-C (0.836 F1, 0.558 mJ) for general use. (3) *Energy-Constrained*: BitNet-Q8PTQ-QMoE (0.801 F1, 0.207 mJ) for edge devices. (4) *Real-Time*: BitNet-Q8/16-PTQ-QMoE-C (0.821 F1, 38 ms std) for timing guarantees.

Comparison to Single Models. MoE architectures show 1-7% lower accuracy than top single models (Q16-Base: 0.859 F1, Q8-Base: 0.858 F1) but offer advantages in interpretability and extensibility. For pure performance, 4-8 bit quantization of monolithic models remains preferable. However, MoE excels for modular updates and continual learning scenarios.

5.4 Inference Latency and Memory Footprint

We benchmark inference latency and peak RAM usage across all configurations. Table 4 presents measurements averaged over ESC-50, Quinn, and UrbanSound8K using 5-fold cross-validation on Apple M3 Max CPU.

Latency-Accuracy Trade-offs. Q1-Base achieves fastest inference (1163 \pm 30 ms, 1.08 \times speedup) despite modest accuracy (0.851 F1), outperforming Q8-Base (1170 ms), Q4-Base (1187 ms), and FP32-Base \dagger (1254 ms). This suggests 1-bit operations benefit from optimized bitwise implementations on Apple M3, avoiding floating-point multiplications. Top F1 models (Q16-Base:

Table 2: Quantization bit-width ablation study across three datasets. Models evaluated using 5-fold cross-validation. Best results per metric and dataset shown in **bold**. “% of 16-bit” represents performance relative to 16-bit baseline.

Bits	Dataset	Params (M)	F1-Score	% of 16-bit	Latency (ms)	Energy (mJ)	RAM (GB)
1	ESC-50	1.2	0.806±0.018	98.3	1103.55±49.50	0.054±0.031	0.85±0.03
		1.2	0.783±0.010	95.5	1117.79±46.82	0.034±0.018	0.84±0.06
		1.2	0.819±0.021	99.9	1126.03±51.66	0.034±0.023	0.86±0.04
		1.2	0.818±0.012	99.8	1098.21±19.35	0.048±0.021	0.93±0.01
		1.2	0.819±0.020	100.0	1459.19±10.58	0.018±0.003	0.95±0.00
2	Quinn	1.2	0.803±0.004	99.8	1197.66±14.50	0.122±0.021	1.34±0.11
		1.2	0.796±0.011	99.0	1195.76±34.13	0.134±0.040	1.33±0.17
		1.2	0.805±0.009	100.1	1199.26±36.43	0.167±0.045	1.26±0.30
		1.2	0.808±0.008	100.4	1209.00±6.67	0.170±0.040	1.09±0.10
		1.2	0.804±0.005	100.0	1129.87±41.36	0.065±0.005	1.32±0.17
4	UrbanSound8K	1.2	0.944±0.009	99.2	1187.49±9.24	0.128±0.025	1.30±0.14
		1.2	0.921±0.010	96.7	1210.45±11.38	0.197±0.051	1.31±0.21
		1.2	0.950±0.008	99.7	1235.90±17.80	0.213±0.033	1.10±0.40
		1.2	0.948±0.010	99.5	1203.95±2.90	0.217±0.066	1.03±0.23
		1.2	0.952±0.006	100.0	1178.25±8.19	0.126±0.038	1.06±0.30

0.859, Q4/Q8-Base: 0.858) exhibit 1170-1256 ms latency, within 7-8% of fastest, indicating framework overhead dominates arithmetic precision for compact 1.2M-parameter models on CPU.

MoE Characteristics and Memory. MoE architectures show 4-17% higher latency than single models, with BitNet-Q4/8/16-QMoE exhibiting $72\times$ larger variance (230 ms std) versus Q8-Base (12 ms std) due to data-dependent routing. Curiosity variants reduce variance to 29-39 ms through epistemic uncertainty-based load balancing. RAM varies 0.86-1.17 GB despite 4 \times parameter differences (1.2-5.0M), confirming peak RAM is dominated by framework overhead rather than weights; even 1GB RAM devices can accommodate our models.

Latency Stability. Curiosity routing improves stability 8 \times : BitNet-Q4/8-QMoE-C (1278±29 ms) versus uniform routing (1335±230 ms), converting bimodal distributions to Gaussian profiles, critical for real-time audio requiring predictable response times.

Deployment Recommendations. (1) *Latency-Critical (<1200ms)*: Q1-Base (1163 ms, 0.851 F1) or Q8-Base (1170 ms, 0.858 F1). (2) *Balanced*: Q4-Base (1187 ms, 0.858 F1). (3) *Maximum Accuracy*: Q16-Base (1256 ms, 0.859 F1). (4) *Memory-Constrained (<900MB)*: BitNet-Q4/8-QMoE-C (1278 ms, 0.86 GB, 0.836 F1). (5) *Stable Real-Time*: Q8-Base (1170±12 ms).

5.5 Statistical Significance Testing

We validate findings using paired t-tests on 5-fold cross-validation scores with Bonferroni correction ($\alpha = 0.05/n$, n = number of comparisons).

Cross-Dataset Generalization. Limited significant differences exist between quantized models and FP32 baseline. Q16-Base significantly outperforms FP32-Base on UrbanSound8K (0.952 vs 0.946 F1, $p=0.022$) and BitNet-Q8/16-PTQ-QMoE-C on Quinn (0.812 vs 0.803 F1, $p=0.021$), but no models significantly exceed baseline on ESC-50. This suggests dataset inter-class separability determines whether quantization maintains statistical parity with full precision.

Quantization Bit-Width Effects. Extreme quantization degrades performance significantly: 2-bit on ESC-50 (0.783 vs 0.819 F1, $p=0.004$) and both 1-bit ($p=0.013$) and 2-bit ($p=0.005$) on UrbanSound8K. However, 4-bit and 8-bit maintain statistical parity with 16-bit across all datasets ($p>0.05$), validating 4-bit as optimal and justifying aggressive quantization for deployment.

Curiosity-Driven Routing Benefits. Curiosity routing maintains accuracy equivalence with uniform routing ($p>0.05$ on ESC-50/UrbanSound8K) while delivering substantial stability gains. Only Quinn shows marginal accuracy improvement ($p=0.021$). Critically, the primary benefit is latency predictability (Section 5.4), 82% variance reduction ($p=0.008$), enabling curiosity variants to preserve accuracy while ensuring reliable real-time infer-

Table 3: Mixture-of-Experts with curiosity-driven routing evaluation. Best results per metric shown in **bold**. MoE uses uniform routing; MoE-C employs Bayesian epistemic uncertainty-based selection.

Model	Type	Params (M)	F1	Latency (ms)	Energy (mJ)	CO ₂ (μg)	Eff
BitNet-Q4/8/16-QMoE	MoE	4.99	0.849±0.010	1335±230	0.621±0.227	228±84	1.37
BitNet-Q8/16-PTQ-QMoE	MoE	4.99	0.820±0.025	1219±69	0.222±0.096	82±36	3.70
BitNet-Q8PTQ-QMoE	MoE	2.59	0.801±0.013	1172±46	0.207±0.101	76±37	3.87
BitNet-Q4/8-QMoE-C	MoE-C	3.80	0.836±0.012	1278±29	0.558±0.145	205±53	1.50
BitNet-Q4/8/16-QMoE-C	MoE-C	4.99	0.834±0.013	1281±35	0.529±0.144	195±53	1.58
BitNet-Q8/16-PTQ-QMoE-C	MoE-C	4.99	0.821±0.020	1251±39	0.281±0.093	103±34	2.93
BitNet-Q8PTQ-QMoE-C	MoE-C	2.59	0.818±0.021	1225±38	0.260±0.108	96±40	3.14

Table 4: Inference latency benchmarks across all models. Evaluated using 5-fold cross-validation, averaged across ESC-50, Quinn, and UrbanSound8K. Best results per metric shown in **bold**. Speedup relative to slowest baseline (BitNet-Q4/8/16-QMoE: 1335ms). †FP32 baseline. ‡INT8 PTQ baseline.

Model	Params (M)	Latency (ms)	Speedup	RAM (GB)	F1-Score
Q1-Base	1.2	1162.90±30.25	1.08	1.16±0.10	0.851
Q8-Base	1.2	1170.39±11.94	1.07	1.02±0.15	0.858
BitNet-Q8PTQ-QMoE	2.59	1171.82±46.48	1.07	1.01±0.22	0.801
Q2-Base	1.2	1174.67±34.09	1.07	1.16±0.16	0.833
BitNet-Base	1.2	1186.44±32.02	1.06	1.16±0.11	0.793
Q4-Base	1.2	1187.06±37.92	1.06	1.07±0.29	0.858
BitNet-Q8/16-PTQ-QMoE	4.99	1218.71±69.24	1.03	1.03±0.25	0.820
BitNet-Q8PTQ-QMoE-C	2.59	1224.91±37.97	1.02	0.95±0.20	0.818
BitNet-Q8/16-PTQ-QMoE-C	4.99	1251.06±38.69	1.00	0.92±0.17	0.821
FP32-Base†	1.19	1254.28±41.57	1.00	1.17±0.19	0.855
Q16-Base	1.2	1255.77±25.10	1.00	1.11±0.20	0.859
Q8-Base-PTQ‡	1.19	1263.82±32.53	0.99	1.08±0.18	0.854
BitNet-Q4/8-QMoE-C	3.8	1277.65±29.36	0.98	0.86±0.13	0.836
BitNet-Q4/8/16-QMoE-C	4.99	1280.99±34.55	0.98	0.89±0.14	0.834
BitNet-Q4/8/16-QMoE	4.99	1335.48±230.47	0.94	0.86±0.21	0.849

ence.

Latency and Variance. Quantized models show non-significant latency reductions versus FP32 (Q1-Base: 1.08×, $p=0.054$), but MoE exhibits highly significant overhead: BitNet-Q4/8/16-QMoE-C +11% ($p<0.001$), BitNet-Q4/8-QMoE-C +10% ($p<0.001$). Our most robust finding concerns variance reduction via Levene’s test: BitNet-Q8/16-PTQ-QMoE-C achieves 82% reduction ($p=0.008$), BitNet-Q8PTQ-QMoE-C 81% ($p=0.010$), and single models 64-69% ($p<0.05$). Uniform MoE shows *higher* variance ($p=0.851$), confirming curiosity-based load balancing essential for predictability.

Effect Sizes and Variability. Narrow confidence intervals (± 0.004 -0.033 F1) indicate high precision. Non-significance of 4-bit vs 16-bit (0.001 F1 difference, $p=0.873$ on ESC-50) demonstrates practical equivalence.

Cohen’s d ranges 0.42-1.24 for significant comparisons (2-bit: $d=1.24$). MoE shows 2-3× higher fold-level variability than single models due to data-dependent routing, but performance rankings remain stable (Spearman’s $\rho=0.89$, $p<0.001$).

Deployment Implications. Statistical analysis confirms: (1) 4-bit/8-bit achieve practical equivalence with full precision, (2) MoE lacks significant accuracy gains but introduces latency overhead, (3) curiosity routing significantly improves stability without accuracy gains, and (4) variance reduction (5-8×) is most robust benefit. This guides practitioners toward Q4/Q8-Base for most deployments, reserving MoE-Curiosity for predictable response time requirements.

Table 5: Selected statistical significance tests. Paired t-tests with Bonferroni correction. * $p<0.05$, ** $p<0.01$, *** $p<0.001$.

Test	Comparison	p-value	Sig.
<i>F1-Score Improvements</i>			
Cross-Dataset	Q16 vs FP32 (Urban8K)	0.022	*
Cross-Dataset	Q8/16-PTQ-C vs FP32 (Quinn)	0.021	*
Ablation	2-bit vs 16-bit (ESC-50)	0.004	**
Ablation	4-bit vs 16-bit (ESC-50)	0.873	ns
<i>Latency Overhead</i>			
MoE vs Q8	Q4/8/16-MoE-C vs Q8-Base	<0.001	***
MoE vs Q8	Q4/8-MoE-C vs Q8-Base	<0.001	***
Speedup	Q1 vs FP32	0.054	ns
<i>Variance Reduction (Levene's test)</i>			
Stability	Q8/16-PTQ-C (82% reduction)	0.008	**
Stability	Q8PTQ-C (81% reduction)	0.010	*
Stability	Q8-Base (68% reduction)	0.030	*

6 Discussion

Our findings challenge conventional wisdom in quantized MoE: while heterogeneity boosts adaptability (e.g., 1-2% F1 gains on Quinn), the primary value lies in stability, not raw accuracy-curiosity routing's 82% variance reduction enables deployment in timing-sensitive applications like autonomous vehicles or hearing aids. Hardware limitations (e.g., Apple M3's INT8 overhead) explain modest speedups, suggesting future work on ASIC-optimized quantizers. Cross-dataset robustness highlights ESC-50's sensitivity to diverse sounds, while UrbanSound8K's tolerance supports aggressive quantization for urban monitoring.

Limitations include single-device (CPU) evaluation; multi-platform testing (e.g., GPU/edge TPUs) could reveal broader gains. We focus on classification - extending to regression or generation tasks remains open. Ethically, our low-carbon focus promotes sustainable AI, but deployment in surveillance raises privacy concerns, mitigated by on-device processing.

7 Conclusion

Our curiosity-driven quantized Mixture-of-Experts advances efficient edge AI by fusing epistemic uncertainty-based routing with heterogeneous quantization, delivering stable, low-carbon models without sacrificing accuracy. By prioritizing epistemic exploration, we pave the way for predictable quantized systems in resource-constrained environments, with practical guidelines for deployment. Future extensions to multimodal tasks could further enhance real-world applicability.

References

Kartikeya Bhardwaj, Chingyi Lin, Anderson Luiz Sartor, and Radu Marculescu. Memory- and communication-aware model compression for distributed deep learning inference on iot. *ACM Transactions on Embedded Computing Systems (TECS)*, 18:1 – 22, 2019.

Leo Anthony Celi. Teaching machines to doubt. *Nature Medicine*, 31, 2025.

Benoit Courty, Victor Schmidt, Sasha Luccioni, Goyal-Kamal, MarionCoutarel, Boris Feld, Jérémie Lecourt, LiamConnell, Amine Saboni, Inimaz, supatomic, Mathilde Léval, Luis Blanche, Alexis Cruveiller, ouminasara, Franklin Zhao, Aditya Joshi, Alexis Bogroff, Hugues de Lavoieille, Niko Laskaris, Edoardo Abati, Douglas Blank, Ziyao Wang, Armin Catovic, Marc Alencon, Michal Stęchły, Christian Bauer, Lucas Otávio N. de Araújo, JPW, and MinervaBooks. mlco2/codecarbon: v2.4.1. Zenodo, 2024. Version v2.4.1.

Jason Cramer, Ho-Hsiang Wu, Justin Salamon, and Juan Pablo Bello. Look, listen, and learn more: Design choices for deep audio embeddings. *ICASSP 2019 - 2019 IEEE International Conference on Acoustics, Speech and Signal Processing (ICASSP)*, pages 3852–3856, 2019.

Nithya Davis and K Suresh. Environmental sound classification using deep convolutional neural networks and data augmentation. *2018 IEEE Recent Advances in Intelligent Computational Systems (RAICS)*, pages 41–45, 2018.

Steven K. Esser, Jeffrey L. McKinstry, Deepika Bablani, Rathinakumar Appuswamy, and Dharmendra S. Modha. Learned step size quantization, 2020.

Chang Gao, Jianfei Chen, Kang Zhao, Jiaqi Wang, and Liping Jing. 1-bit fqt: Pushing the limit of fully quantized training to 1-bit, 2024.

Andrey Guzhov, Federico Raue, Jörn Hees, and Andreas Dengel. Audioclip: Extending clip to image, text and audio, 2021.

Nicolás Hernández, Francisco Almeida, and Vicente Blanco. Optimizing convolutional neural networks for iot devices: performance and energy efficiency of quantization techniques. *Journal of Supercomputing*, 80(9):12686 – 12705, 2024. Cited by: 0; All Open Access, Hybrid Gold Open Access.

Shawn Hershey, Sourish Chaudhuri, Daniel P. W. Ellis, Jort F. Gemmeke, Aren Jansen, R. Channing Moore, Manoj Plakal, Devin Platt, Rif A. Saurous, Bryan Seybold, Malcolm Slaney, Ron J. Weiss, and Kevin W. Wilson. Cnn architectures for large-scale audio classification. *2017 IEEE International Conference on Acoustics, Speech and Signal Processing (ICASSP)*, pages 131–135, 2016.

Andrew Howard, Mark Sandler, Grace Chu, Liang-Chieh Chen, Bo Chen, Mingxing Tan, Weijun Wang, Yukun Zhu, Ruoming Pang, Vijay Vasudevan, et al. Searching for mobilenetv3. In *Proceedings of the IEEE/CVF international conference on computer vision*, pages 1314–1324, 2019.

Itay Hubara, Matthieu Courbariaux, Daniel Soudry, Ran El-Yaniv, and Yoshua Bengio. Quantized neural networks: Training neural networks with low precision weights and activations. *J. Mach. Learn. Res.*, 18:187:1–187:30, 2016.

Benoit Jacob, Skirmantas Kligys, Bo Chen, Menglong Zhu, Matthew Tang, Andrew Howard, Hartwig Adam, and Dmitry Kalenichenko. Quantization and training of neural networks for efficient integer-arithmetic-only inference. In *Proceedings of the IEEE conference on computer vision and pattern recognition*, pages 2704–2713, 2018.

Omar Kaziha and Talal Bonny. Exploring quantization-aware training on a convolution neural network. In *2020 International Conference on Communications, Computing, Cybersecurity, and Informatics (CCCI)*, pages 1–5, 2020.

Alex Kendall and Yarin Gal. What uncertainties do we need in bayesian deep learning for computer vision? In *Advances in Neural Information Processing Systems*. Curran Associates, Inc., 2017.

Hoseung Kim, Kwangbae Lee, and Dongkun Shin. Towards accurate low bit dnns with filter-wise quantization. In *2020 IEEE International Conference on Consumer Electronics - Asia (ICCE-Asia)*, pages 1–4, 2020.

Kangkang Liu and Ningjiang Chen. Ptq-so: A scale optimization-based approach for post-training quantization of edge computing. In *2024 27th International Conference on Computer Supported Cooperative Work in Design (CSCWD)*, pages 2078–2083, 2024.

Shuming Ma, Hongyu Wang, Lingxiao Ma, Lei Wang, Wenhui Wang, Shaohan Huang, Lifeng Dong, Ruiping Wang, Jilong Xue, and Furu Wei. The era of 1-bit llms: All large language models are in 1.58 bits. *arXiv preprint arXiv:2402.17764*, 1 (4), 2024.

Annamaria Mesaros, Toni Heittola, Emmanouil Benetos, Peter Foster, Mathieu Lagrange, Tuomas Virtanen, and Mark D. Plumbley. Detection and classification of acoustic scenes and events: Outcome of the dcase 2016 challenge. *IEEE/ACM Transactions on Audio, Speech, and Language Processing*, 26:379–393, 2018.

Sangyun Oh, Hyeonuk Sim, Joungyun Kim, and Jongeun Lee. Non-uniform step size quantization for accurate post-training quantization. *Lecture Notes in Computer Science (including subseries Lecture Notes in Artificial Intelligence and Lecture Notes in Bioinformatics)*, 13671 LNCS:658 – 673, 2022. Cited by: 8.

S. A. C. Ordoñez. Humility and curiosity in human–ai systems for health care. *The Lancet*, 406, 2025.

Deepak Pathak, Pulkit Agrawal, Alexei A. Efros, and Trevor Darrell. Curiosity-driven exploration by self-supervised prediction. In *Proceedings of the 34th International Conference on Machine Learning - Volume 70*, page 2778–2787. JMLR.org, 2017.

Svetlana Pavlitskaya and Stefan Harmeling. Evaluating mixture-of-experts architectures for network aggregation. In *Pattern Recognition. DAGM GCPR 2022. Lecture Notes in Computer Science*, pages 136–149. Springer, 2022.

Karol J Piczak. Esc: Dataset for environmental sound classification. In *Proceedings of the 23rd ACM international conference on Multimedia*, pages 1015–1018, 2015.

Joan Puigcerver, Carlos Riquelme, Basil Mustafa, Maxim Neumann, and Neil Housby. From sparse to soft mixtures of experts. In *International Conference on Learning Representations (ICLR 2024)*, 2024.

Colin A Quinn, Patrick Burns, Gurman Gill, Shrishail Baligar, Rose L Snyder, Leonardo Salas, Scott J Goetz, and Matthew L Clark. Soundscape classification with convolutional neural networks reveals temporal and geographic patterns in ecoacoustic data. *Ecological Indicators*, 138:108831, 2022.

Carlos Riquelme, Joan Puigcerver, Basil Mustafa, Maxim Neumann, Rodolphe Jenatton, and Neil Housby. Scaling vision with sparse mixture of experts. In *Proceedings of the 38th International Conference on Machine Learning (ICML 2021)*, pages 8747–8760. ACM, 2021.

Justin Salamon, Christopher Jacoby, and Juan Pablo Bello. A dataset and taxonomy for urban sound research. In *Proceedings of the 22nd ACM international conference on Multimedia*, pages 1041–1044, 2014.

Anubhav Sharma and Ramesh C. Tripathi. A flexible probabilistic framework for large-margin mixture of experts. *Machine Learning*, 108(7):1213–1242, 2019.

Sameh Souli and Zied Lachiri. Audio sounds classification using scattering features and support vectors machines for medical surveillance, 2018.

S. S. Stevens, J. Volkmann, and E. B. Newman. A scale for the measurement of the psychological magnitude pitch. *The Journal of the Acoustical Society of America*, 8(3):185–190, 1937.

Mingxing Tan and Quoc Le. Efficientnet: Rethinking model scaling for convolutional neural networks. In *International conference on machine learning*, pages 6105–6114. PMLR, 2019.

Antonio J. Torija, Diego P. Ruiz, and Ángel F. Ramos-Ridao. A tool for urban soundscape evaluation applying support vector machines for developing a soundscape classification model. *Science of The Total Environment*, 482–483:440–451, 2014.

Tal Zeevi, Lawrence H Staib, and John A Onofrey. Enhancing uncertainty estimation in semantic segmentation via monte-carlo frequency dropout. In *2025 IEEE 22nd International Symposium on Biomedical Imaging (ISBI)*, pages 1–5. IEEE, 2025.

Yongchao Zhou, Natalia Neverova, Sam Gross, and Mike Rabat. Mixture-of-experts with expert choice routing. In *Advances in Neural Information Processing Systems (NeurIPS 2022)*, 2022.

Supplementary Material

A Carbon Emissions Analysis

We provide detailed carbon emission measurements using CodeCarbon [Courty et al. \(2024\)](#) during training and validation on Apple M3 Max CPU (36GB RAM). Table 6 presents emission data for all model configurations.

A.1 Training vs. Deployment Emissions

Single models (1.2M params) emit 22.8 to 55.0 μg CO_2 during training, while MoE architectures (2.6 to 5.0M params) produce 77.6 to 230.6 μg . However, deployment emissions dominate at scale. For 1M daily inferences over 1 year (grid: 367 g CO_2/kWh), FP32-Base training emits 22.8 μg but deployment produces 2.4 g/year, a 105,000 \times increase. Q4-Base shows similar patterns: 52.3 μg training versus 4.6 g/year deployment. This demonstrates that deployment emissions dominate by approximately 10,000 \times for models serving more than 1,000 inferences.

A.2 Green AI Recommendations

Based on our analysis: (1) Use FP32/Q16 for prototyping (23-28 $\mu\text{g}/\text{experiment}$); (2) Deploy Q4/Q8 for production to minimize long-term emissions; (3) Schedule training during low-carbon grid hours for 2-5 \times reduction; (4) Train once and fine-tune for multiple tasks to amortize carbon costs.

B Model Size Analysis

Table 7 presents model sizes across all quantization schemes. Q8-Base-PTQ achieves highest compression (15.65 \times) through bitwise operations, while Q1-Base reaches 19.99 \times via BitLinear quantization.

B.1 Optimal Configuration

Q4-Base represents the optimal deployment point with 7.03 \times compression (687 KB) and 0.858 F1 score, within 0.1% of 16-bit performance while consuming 41% less energy than 8-bit. This balance makes it suitable for most edge deployment scenarios.

B.2 MoE Trade-offs

MoE models show negative compression (0.85 \times) due to multiple expert networks. BitNet-Q4/8/16-QMoE contains 5.67 MB versus single models' <1.3 MB. How-

Table 6: Carbon emissions during training. \dagger FP32 baseline. \ddagger INT8 PTQ baseline.

Model	P. (M)	CO_2 (μg)	Rate ($\mu\text{g}/\text{s}$)	F1
FP32 \dagger	1.19	22.8\pm5.0	0.96 \pm 0.27	0.855
Q8-PTQ \ddagger	1.19	25.9 \pm 17.3	1.01 \pm 0.80	0.854
Q16	1.2	27.5 \pm 8.3	0.87\pm0.35	0.859
Q1	1.2	38.8 \pm 9.6	1.06 \pm 0.34	0.851
Q2	1.2	46.4 \pm 14.3	1.08 \pm 0.45	0.833
BitNet	1.2	48.1 \pm 19.0	1.04 \pm 0.57	0.793
Q4	1.2	52.3 \pm 12.8	1.05 \pm 0.40	0.858
Q8	1.2	55.0 \pm 16.9	1.05 \pm 0.44	0.858
Q8PTQ-MoE	2.59	77.6 \pm 37.1	1.09 \pm 0.74	0.801
Q8/16PTQ-MoE	4.99	83.6 \pm 35.5	1.10 \pm 0.64	0.820
Q8PTQ-MoE-C	2.59	97.6 \pm 39.8	1.04 \pm 0.61	0.818
Q8/16PTQ-MoE-C	4.99	105.2 \pm 34.4	1.05 \pm 0.51	0.821
Q4/8/16-MoE-C	4.99	196.8 \pm 53.1	1.06 \pm 0.41	0.834
Q4/8-MoE-C	3.8	207.5 \pm 53.2	1.11 \pm 0.40	0.836
Q4/8/16-MoE	4.99	230.6 \pm 83.5	1.09 \pm 0.56	0.849

ever, MoE architectures enable dynamic precision routing, modular updates, and interpretability. For applications prioritizing minimal memory footprint, single quantized models (Q4/Q8-Base) remain superior. MoE is appropriate when interpretability or continual learning are critical.

Table 7: Model sizes under different quantization schemes.

Model	Quant.	Bits	Params	KB	MB	Red.
FP32	None	32	1,206,770	4,830.8	4.83	1.00 \times
Q1	BitLinear	1	1,211,122	241.6	0.24	19.99 \times
Q2	BitLinear	2	1,211,122	390.1	0.39	12.38 \times
Q4	BitLinear	4	1,211,122	687.1	0.69	7.03 \times
Q8	BitLinear	8	1,211,122	1,281.0	1.28	3.77 \times
Q16	BitLinear	16	1,211,122	2,468.8	2.47	1.96 \times
BitNet	Ternary	2	1,211,122	393.9	0.39	12.26 \times
Q8-PTQ	Bitwise	2	1,205,760	308.6	0.31	15.65 \times
MoE	Hetero.	Mix	1,415,687	5,669.8	5.67	0.85 \times
MoE-C	H.+Bay.	Mix	1,415,687	5,669.8	5.67	0.85 \times